Proceedings of the
Annual Stability Conference
Structural Stability Research Council
Louisville, Kentucky, April 2-4, 2025

Global Buckling Measurement in Steel Decks using Fiber Optic Sensing, Infrared Optical Tracking, and Point Clouds

Monamy Mustaq[1],Gowshikan Arulananthan[2], Richa Dutta Rakhee [3], Nate Opperman[4], Hyeyoung Koh[5], Qiquan Xiong[6], Jesse C. Hampton[7], Hannah B. Blum[8]

Abstract

Quantification of global buckling behavior of steel systems is crucial to determine accurate load capacities of structural steel systems. New forms of instrumentation permit a robust method for obtaining global behavior during both laboratory studies and field investigations. This paper explores global buckling quantification from various forms of instrumentation meant to capture multiscale strain behavior, including distributed fiber optic sensing, infrared optical tracking, and point clouds obtained from photogrammetry and LiDAR (Light Detection and Ranging) scans. The test case is a profiled steel deck loaded with uniform pressure using a 2.4 m (8 ft.) by 4.9 m (16 ft.) by 0.9 m (3 ft.) vacuum box. Two different experimental layouts were considered, a two-span deck with a center support, and a single-span deck. The OptiTrack system used infrared optical tracking to measure 3D displacements. The Scaniverse app on an Apple iPad Pro scanned using LiDAR and photogrammetry and converted the scans to a low-density point cloud, which was used to determine vertical displacements. The vertical displacements measured by the OptiTrack system and the Scaniverse app were compared. Distributed fiber optic sensing provided continuous longitudinal strain measurements along the deck flanges which illustrated the overall deck behavior through the strain profile along the longitudinal direction. A method to integrate the distributed strain from multiple systems to out-of-plane displacements is presented. The findings of this study are expected to contribute to the development of innovative solutions using advanced measurement techniques for global buckling measurement.

[1]Graduate Research Assistant, University of Wisconsin Madison, <mustaq@wisc.edu>
[2]Graduate Research Assistant, University of Wisconsin Madison, <arulananthan@wisc.edu>
[3]Graduate Research Assistant, University of Wisconsin-Madison <rakhee@wisc.edu>
[4]Graduate Research Assistant, University of Wisconsin Madison, <nopperman@wisc.edu>
[5]Assistant Professor, Washington State University (Formerly Postdoctoral Associate at the University of Wisconsin-Madison), Pullman, WA, <hyeyoung.koh@wsu.edu>
[6]Research Scientist, University of Wisconsin-Madison, <qxiong26@wisc.edu>
[7]Assistant Professor, University of Wisconsin-Madison, <jesse.hampton@wisc.edu>
[8]Alain H. Peyrot Associate Professor, University of Wisconsin-Madison, <hannah.blum@wisc.edu>

1 Introduction

Steel deck, formed from a thin-walled corrugated sheet of cold-formed steel, is widely utilized as a structural component in construction, primarily serving as formwork or a structural base for floors, roofs, or composite slabs. Steel decks also provide essential structural functions, such as being used as diaphragms to distribute lateral loads and improve overall structural stability. These lateral loads such as wind and seismic loads are predominantly uniform in distribution.

However, during experimental assessments of steel deck capacity John et al. (2020) , Raebel and Gwozdz (2020), Lawson and Popo-Ola (2013), a spreader beam is often used to apply point loads. Application of such point loads can create concentrated stress in localized areas, which can lead to deformation or elastic buckling. Since steel deck is mostly subjected to uniform loading, application of point load in an experimental setup does not simulate the actual loading condition. To address this issue, a new vacuum box chamber called SEAhorse (Suction Experimental Apparatus) was used. Uniform pressure loading was produced in vacuum box by creating negative pressure inside the box by suctioning air out of the box. This uniform pressure across the deck surface can represent a distributed gravity load. This vacuum box has been used to assess the capacity of steel deck systems and to explore its buckling behavior.

Buckling is a structural phenomenon that occurs when a structural component suddenly deforms under a compressive load. Even though cold formed steel members may also be susceptible to distortional buckling along with global and local buckling modes, only global buckling mode is explored in this study. Global buckling refers to a structural failure mode where a structure or major component suddenly deforms significantly under compressive load, essentially buckling as a whole rather than just a localized area. It often leads to catastrophic failure as it causes the overall instability of the structure, compared to local buckling which affects smaller sections of the member.

Several research studies have been conducted on measuring global buckling capacity of steel deck systems, including experimental and computational studies. For experimental studies, displacement transducers He et al. (2023), LVDTs and strain gauges Liang et al. (2024) are most used to measure global buckling capacity of steel deck systems. Conventional methods of measuring global buckling capacity have their own limitations such as limited gauge length or measurements at discrete points. This study explores new forms of instrumentation to measure global buckling capacity of steel deck systems. To detect global buckling of steel deck, distributed fiber optic sensing and optical tracking system were employed. Point cloud scans of the steel deck were obtained using photogrammetry and LiDAR, to determine vertical displacements. The outcome of this study will contribute to the development of innovative sensing techniques to measure global buckling capacity.

2 Test Setup

2.1 Vacuum Box

The vacuum box, constructed from wood panels, is an 8-foot (2.4 m) by 16-foot (4.9 m) structure with a height of 3 feet (0.9 m), as shown in Figure 1. To ensure structural integrity during testing, the box was securely bolted to the floor. The box comprises modular 4-foot (1.2 m) sections,

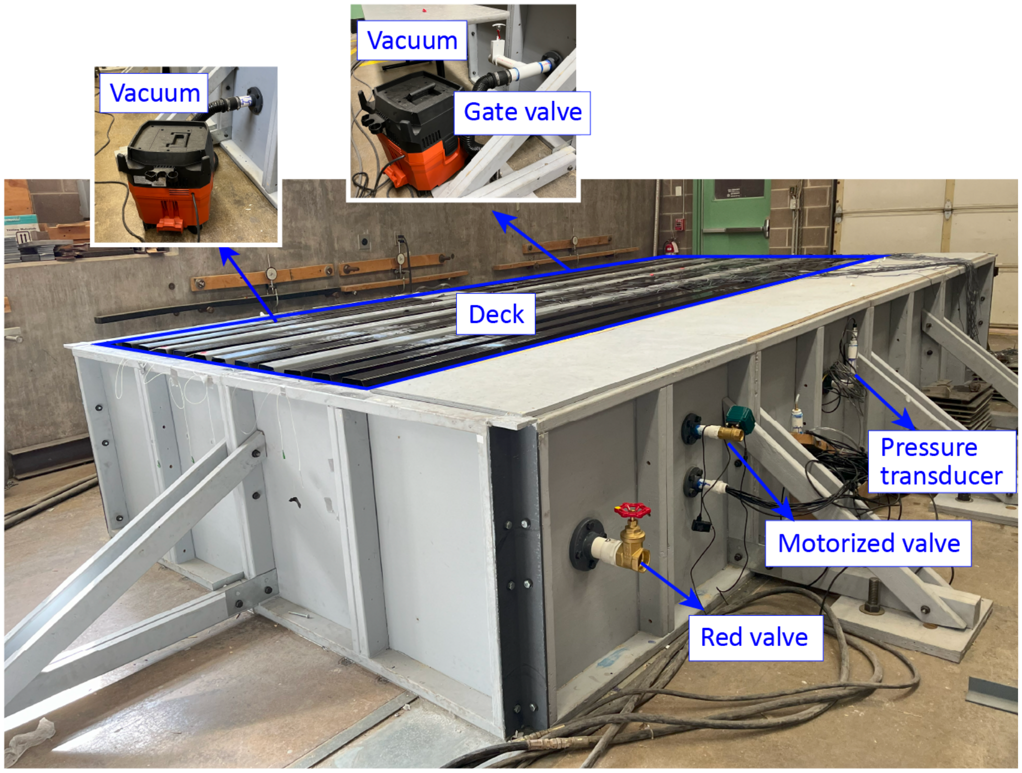

Figure 1: The Vacuum Box

allowing its size to be adjusted for future testing requirements. Three valves were used to siphon air out of the box during test, including the Gate valve, the Motorized valve, and the Red valve. A pressure transducer has been used to measure pressure inside the box. Several flanges were installed along the sides of the box to route cables from the instrumentation inside the box to outside. A plastic tarp was used to cover the top of the box. The tarp was secured with double-sided tape along the top edges of the box, ensuring a proper vacuum seal was maintained throughout the test.

2.2 Test Setup

A 22 gauge wide rib roof deck (1.5WR22), was tested with the vacuum box. The deck profile is shown in Figure 2. Three test setups were used with different support conditions. For the first test, DT1 (deck test 1), two 3-foot (0.9 m) by 16-foot (4.9 m) decks were placed along the longitudinal edge of the vacuum box. The plane profile of the specimen is 6-foot (1.8 m) wide and 16-foot (4.9 m) long. The decks are simply supported at the center and 8 inches (203 mm) in from the deck edges. For the second test, DT2 (deck test 2), deck profile is same as the first one, 6-foot (1.8 m) wide and 16-foot (4.9 m) long. The decks are supported at 24 inches (608 mm) in from both edges. For the third test, DT3 (deck test 3), two 3-foot (0.9 m) by 14-foot (4.9 m) decks were used, giving a specimen profile of 6 foot (1.8 m) wide and 14 foot (4.2 m) long. The decks were simply supported at 12 inches (304 mm) on both sides from the edge of the deck. The first test setup gives two spans of 7.33 ft (2.33 m) while the second and third test setup give one single span of 12 ft (3.65 m) (Figure 3).

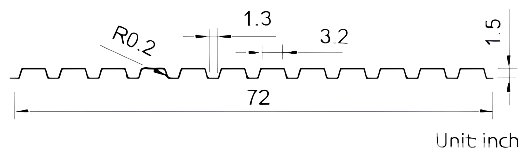

Figure 2: 1.5WR22 deck profile

(a) Deck span with middle support-DT1

(b) Deck span without middle support-DT2 and DT3

Figure 3: Test Setup

The same deck profile was used for all three tests, with a depth of 1.5-inch (38 mm), a top flange width of 3.2-inch (81 mm), a bottom flange width of 1.3-inch (33 mm), a corner radius of 0.2-inch (5 mm), and a thickness of 0.03-inch (0.76mm). Screws were used to attach the bottom flanges of the deck profile to the supports. Plywood was used to fill the remaining space to the box edge.

Standard tensile coupon of 7.87 inch (2 m) long and 0.75 inch (0.19m) wide according to ASTM E8 ASTM E8/E8M-13a (2015), was cut from the top flange of the deck material. The coupon had a nominal yield strength of 80 ksi (550 MPa), nominal ultimate strength 82 ksi (565 MPa) and nominal elastic modulus of 29,500 ksi (203 GPa). Two coupon specimens were tested to get the material properties of the steel deck. For the first specimen, a 5 mm strain gauge was affixed at the mid-length of the coupon to measure strain response. In the second specimen, both a 50 mm extensometer and a 5 mm strain gauge were attached symmetrically on either side of the coupon at its mid-length. The loading rate used for these experiments, was obtained by following the methodology of Huang and Young Huang and Young (2014). Figure 4 shows the resulting stress-strain curves, where F_y represents the yield strength, F_u is the ultimate tensile strength, E is the Young's modulus. The average material properties obtained from the three test cases are : E = 25,636 ksi, F_y = 77.73 ksi, and F_u = 82.56 ksi.

2.3 Test Procedure

Three valves known as the Gate valve, the Red valve, and the Motorized valve and two vacuums were used to apply pressure load to the decks. The experiment started with all the valves open and turning on the vacuums. Pressure was incrementally increased by closing the valves in a predetermined sequence, ensuring controlled and gradual loading. After the desired pressure is achieved and the test is completed, all valves were opened to release the pressure, and vacuums were turned off.

The pressure rate for each test is shown in Figure 5. For first test setup, the test was concluded when a maximum desired pressure of 100 psf (4.8 kPa) was achieved. For second and third test setup, the deck was loaded until failure, with a maximum recorded pressure of 58 psf (2.78 kPa) and 39 psf (1.87 kPa) respectively. During the third test, the test was paused twice to record point cloud scans, when the pressure reached approximately 18 psf (0.86 kPa) and 38 psf (1.82 kPa).

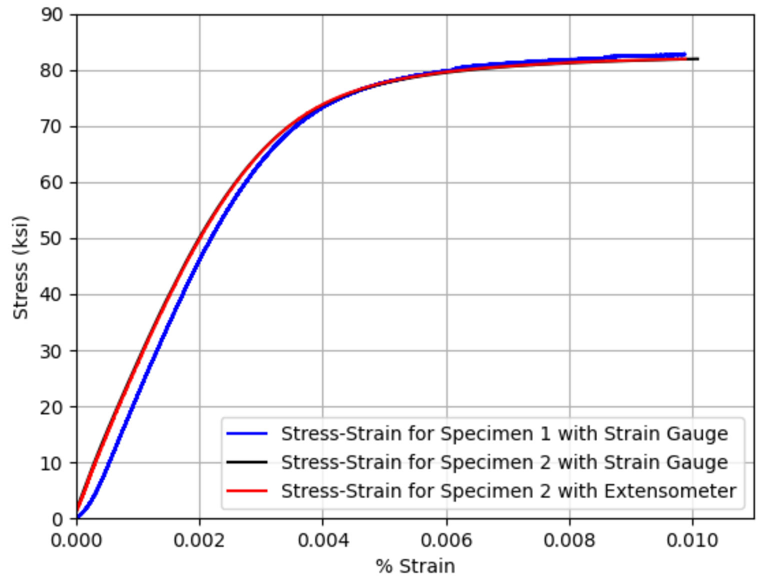

Figure 4: Stress Strain Curve

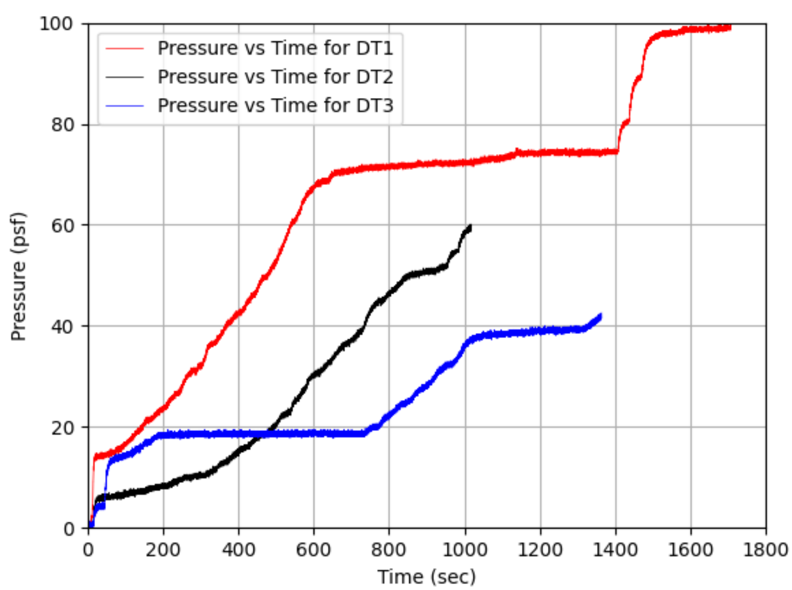

Figure 5: Pressure Loading for each test

2.4 Instrumentation

To measure the global buckling capacity of steel deck, fiber optic sensing, conventional strain gauges, optical tracking were employed. Moreover, point cloud scans were taken to measure displacement of the deck. The instrumentation layout for each test is shown in Figure 6, 7 and 8.

2.4.1 Distributed Fiber Optic Sensing

Distributed Fiber Optic Sensing (DFOS) has rapidly evolved as an advanced sensing technology, offering significant advantages over traditional sensors such as electrical strain gauges. The insensitivity of fiber optic sensors to electrical and electromagnetic disturbances, coupled with their robust and durable nature, has positioned DFOS as a reliable solution for Structural Health Monitoring (SHM) applications (Rajan and Prusty (2016)). Additionally, their capability to provide continuous, distributed measurements has significantly contributed to their growing adoption in monitoring the health and integrity of civil infrastructure.

DFOS is based on examining the characteristics of the backscattered light spectrum in the fiber optic cable (Kechavarzi et al. (2016)). When light travels through an optical fiber, a portion of its power is scattered due to interactions with impurities and structural irregularities in the fiber core. Scattering is also influenced by environmental factors such as strain and temperature variations. The frequency and amplitude of the backscattered light are analyzed to detect these changes. The DFOS technique used in this study is based on the Rayleigh backscattering phenomenon.

This study employed the LUNA ODiSI 6100, a Rayleigh-based Optical Frequency Domain Reflectometry (OFDR) DFOS system, to perform distributed strain measurements. A spatial resolution of 1.3 mm was chosen for this experiment. Spatial resolution is the smallest length over which the system can accurately measure strain or temperature. OFS PEEK-coated single-mode fibers were used in this study. The fibers were attached (Fig. 9) to the top surface of the deck at a number of top and bottom flanges as shown in the instrumentation layout (Fig. 6, 7 and 8) using M-Bond 200 adhesive. The first letter in the instrumentation tag indicates the equipment type, with F for fiber optic cable and S for strain gauge. The second letter denotes the direction to which equipment was installed, in this case L for longitudinal. The third letter specifies the location of flange being instrumented, T for top flange and B for bottom flange. The last number is the instrument number for fiber or strain gauge.

2.4.2 Optical Tracking System

Optical tracking is a method to track and capture the motion of small retroreflective markers attached to an object and delivers real time motion data. The position of the retroreflective markers are determined by using a multiple camera systems. This vision based method has been used for structural health monitoring such as structural deformation measurement Park et al. (2015); Kalybek, Bocian, and Nikitas (2021). In this study, to capture the movement of the deformed deck caused by increasing pressure load, the Optitrack system was employed. Motive 3.0.2 software Optitrack (2021) was used to track the real time position of the retroreflective markers. By pairing Motive software with OptiTrack cameras, accuracy of up to 0.1 mm can be achieved, depending on the test calibration. In this study, OptiTrack system was calibrated with the accuracy of 0.1 mm for the first test setup, 3 mm for the second test setup and 0.405 mm for the third test setup. Markers

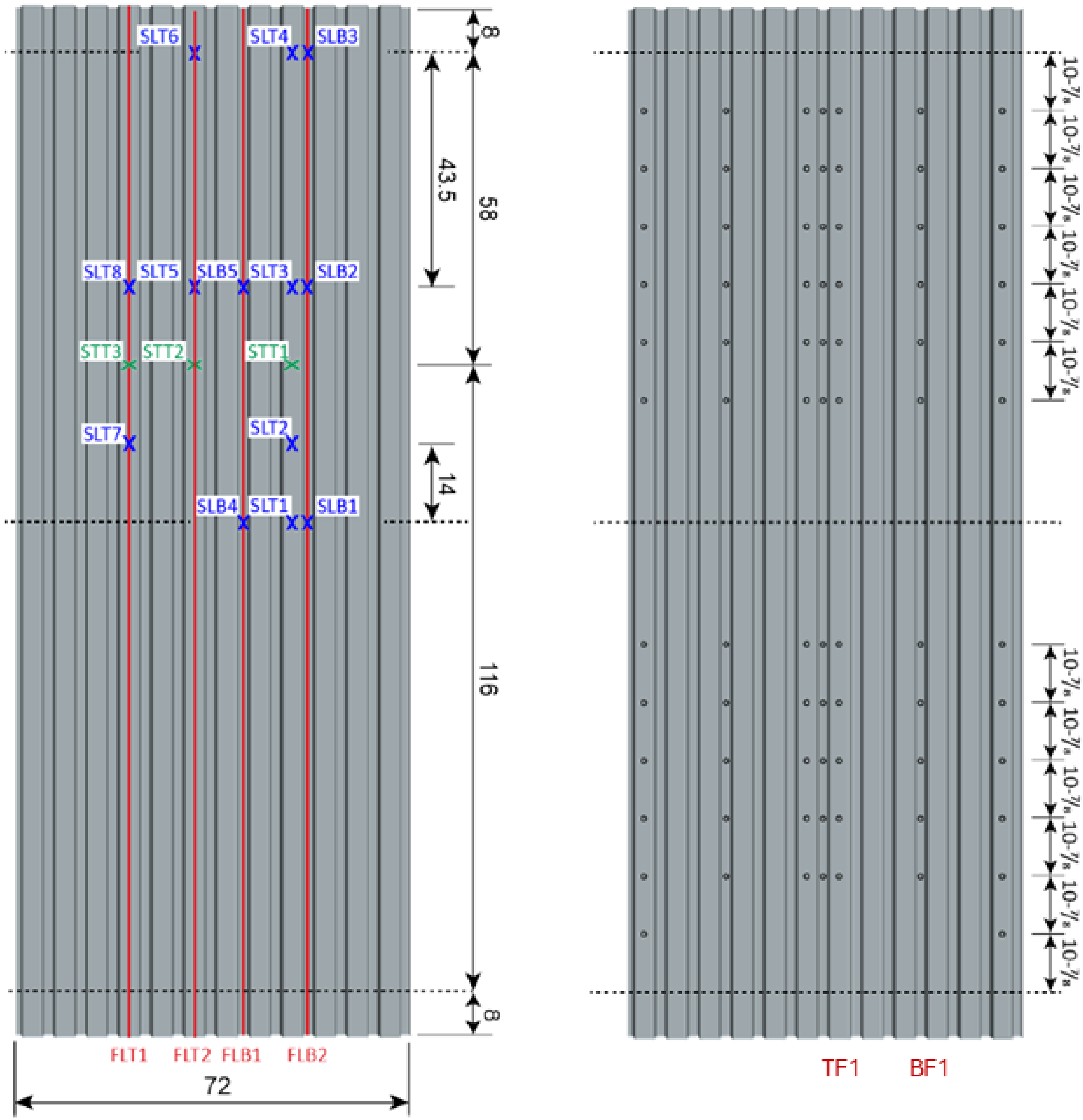

Figure 6: Test DT1

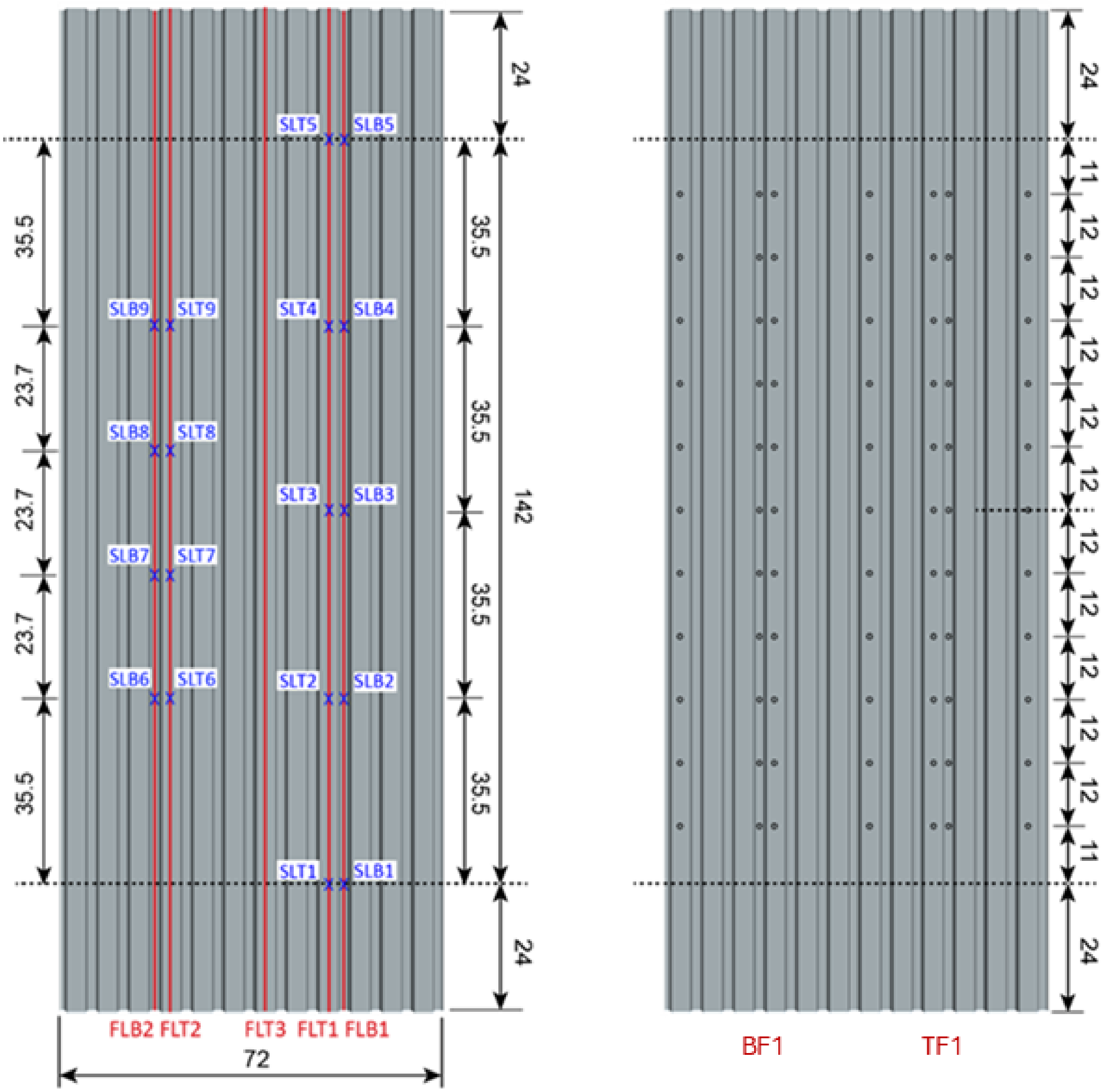

Figure 7: Test DT2

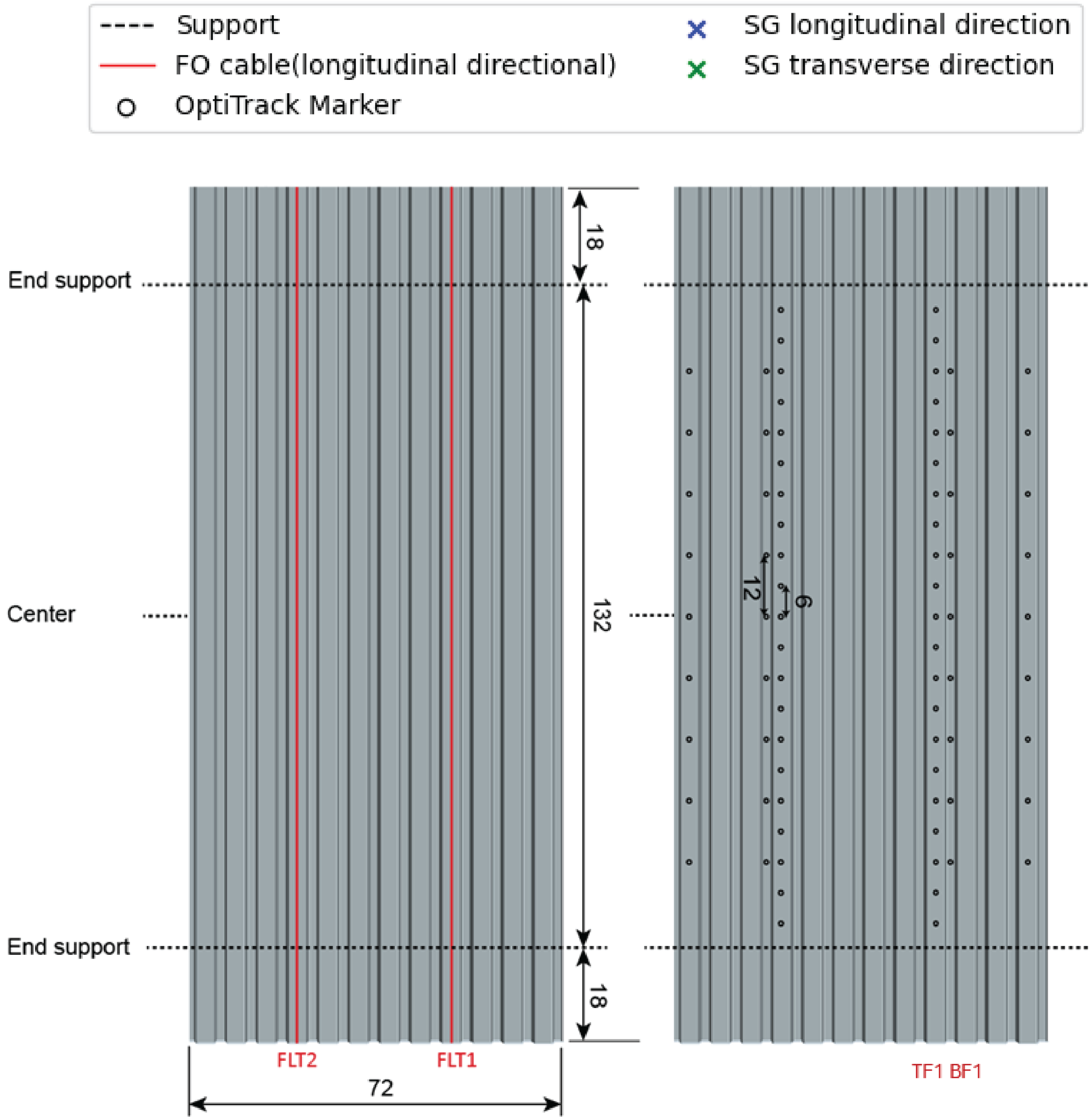

Figure 8: Test DT3

Figure 9: Fiber Optic Cable and Strain Gauges installed for first test DT1

were installed on the underside of the deck specimen as a dark environment was needed for the infrared cameras to prevent light reflection interference. OptiTrack cameras were placed on the floor inside of the box. A total of eight cameras were used for each test setup in this study. The underside of the deck was painted matte black to reduce light reflections as the steel deck surface is shiny and reflective and it can create interference for the cameras. The OptiTrack setup is shown in Figure 10.

For the first test setup, seventy-nine markers were attached to the underside of four top flanges and three bottom flanges. For the second test, seventy-four markers were attached to the underside of five top flanges and two bottom flanges. For the third test setup, seventy-seven markers were attached to the underside of two top flanges and four bottom flanges. Markers were positioned along the deck spans between the supports. Due to the presence of supports underneath the deck specimen, markers were not able to be placed in those support positions.

2.4.3 Point Cloud

Point cloud scanning refers to the process of capturing 3D data points using technologies like laser scanning, LiDAR, or photogrammetry. The resulting file format is a point cloud, which represents the shape of a physical object in 3D space through the 3D positions of many densely spaced points. Point cloud scanning has been previously used for structural health monitoring Chen et al. (2012)) and displacement measurement of structures (Jo et al. (2018)). In this study, LiDAR (Light Detection and Ranging) system has been used to measure global buckling capacity of the steel deck. LiDAR is a remote sensing technology that uses laser beams to measure precise 3D coordinates. LiDAR system emits pulsed laser light into the structure. These pulses, traveling at the speed of light, bounce off surrounding objects and return to the LiDAR sensor. The sensor measures the

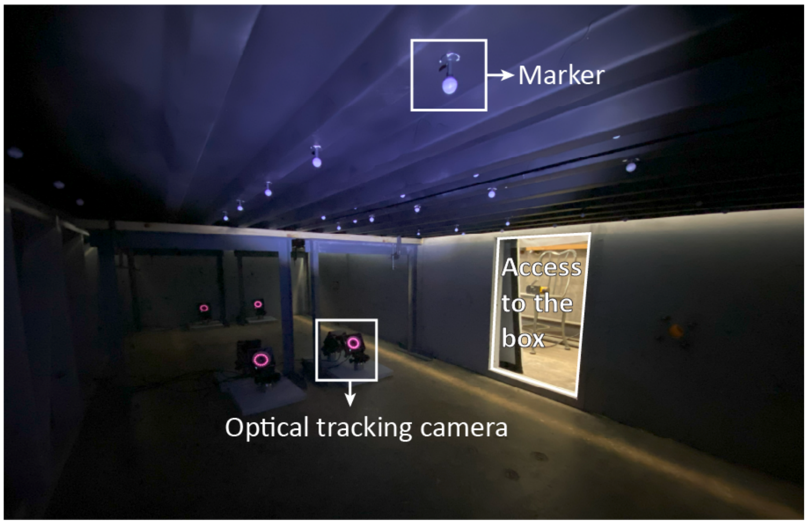

Figure 10: Optical Tracking Camera and Markers installed on the underside of the deck

time that it took for each pulse to return and calculates the distance that it traveled. As the speed of laser light is constant, this “time of flight” can be used to calculate precise distances. By repeating the process and sending out laser pulses across a larger area, time-of-flight measurements can be collected on billions of individual points and processed in real time into what is known as a LiDAR point cloud.

An Artec Ray Scanner and An Apple iPad Pro (6th generation, 12.9 in.) equipped with a LiDAR camera were employed to assess global buckling in the third test setup. The Artec Ray Scanner captured the initial, unloaded deck with a range accuracy of 1 mm + 10 micrometers per million. For the Apple iPad Pro, the Scaniverse Scaniverse Inc. (2024) app was used for scanning the deformed deck during testing. Scaniverse offers a centimeter level accuracy for 3D point cloud generation. Scans were taken using the Scaniverse app twice during the third testing, when pressure was approximately 18 psf (0.86 kPa) and 38 psf (1.82 kPa).

3 Results

Uniform pressure load was applied to the decks according to the procedure mentioned in Section 2.3 for the two test setups mentioned. For test setup DT1, the test was completed when pressure reached close to the target pressure of 100 psf. A photo of the deformed deck with evidence of local buckling is shown in 11. After opening the gates and turning off the vacuums, the deck returned to its initial position.

For DT2 and DT3, the test was completed upon the failure of the deck. The maximum recorded pressure during the experiment was 58 psf and 39 psf, respectively. Photos of the deformed decks are shown in Figure 11. The overall deck deformations are visible in addition to local buckling in the top flanges.

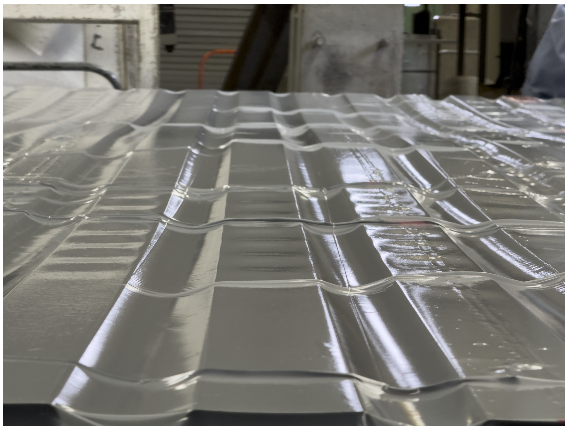

(a) Test DT1

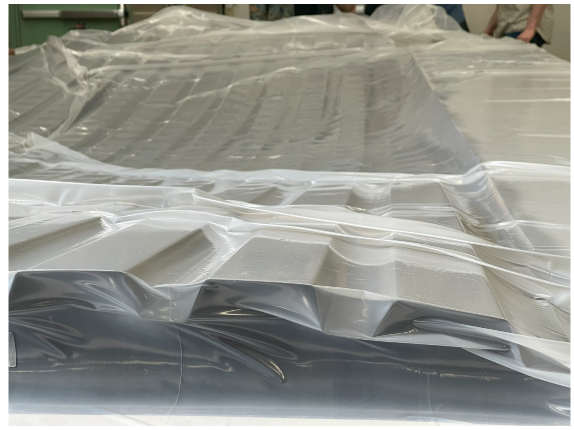

(b) Test DT2

(c) Test DT3

Figure 11: Deformed Deck during testing

3.1 Strain Results

Figure 12 and Figure 13 provide the strain results measured by the strain gauges at the bottom flange. For the first test DT1, total of five strain gauges were installed on the two bottom flanges. SLB1 and SLB4 are positioned at the center support (Figure 6). Both SLB1 and SLB4 exhibit compressive strain throughout the pressure range due to the negative bending moment at the center support, consistent with the expected bending moment diagram of a double-span beam. SLB2 and SLB5 are positioned at the midpoint (Figure 6) between the center support and the end support, show tensile strain, aligning with positive bending moments. SLB3 at the end support shows minimal compressive strain. For the second test (DT2), nine strain gauges were strategically installed along the two bottom flanges to accurately capture the strain distribution. SLB1 and SLB5 are positioned at the end supports (figure 7), hence they exhibit compressive strain. The rest of the strain gauges which are positioned along the span between the end supports, exhibit tensile strain, indicating that the bottom flange is experiencing tension due to the positive bending moment. SLB3 exhibits a maximum magnitude of tensile strain as it is positioned at the midpoint of the span, as this is where the bending moment reaches its peak in a single-span beam subjected to uniform or concentrated loading. This confirms the expected pattern of the bending moment diagram, where sagging moments dominate, causing the bottom flange to stretch while the top flange experiences compression. Most of the strain gauges were installed as close as possible to the fiber cables for both tests.

Distributed fiber optic sensing captures multiscale strain behavior, including global buckling be-

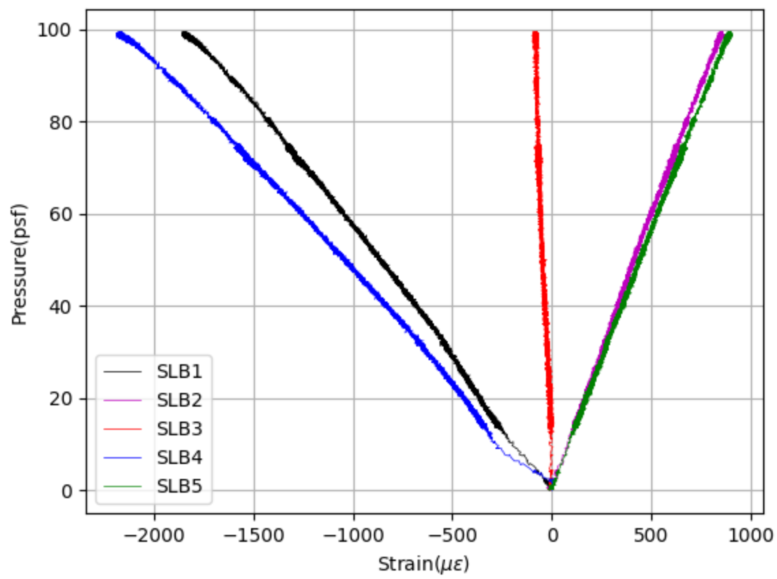

Figure 12: Strain profile of bottom flanges for DT1

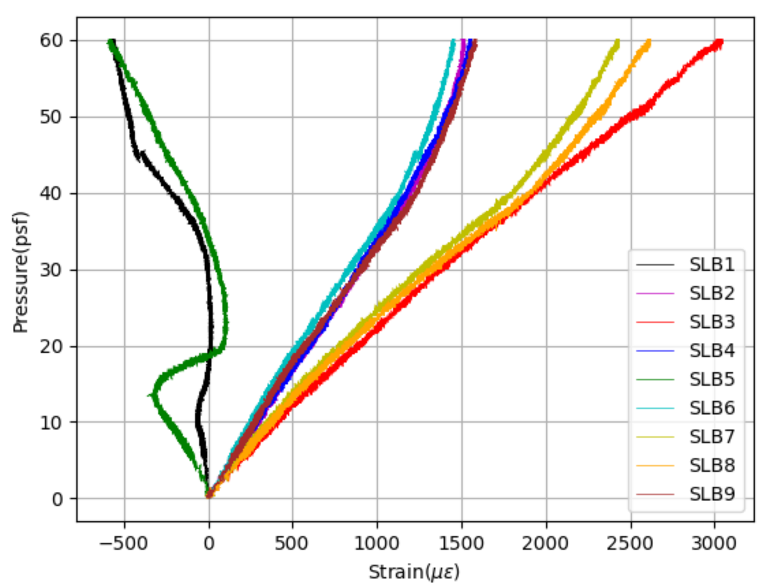

Figure 13: Strain profile of bottom flanges for DT2

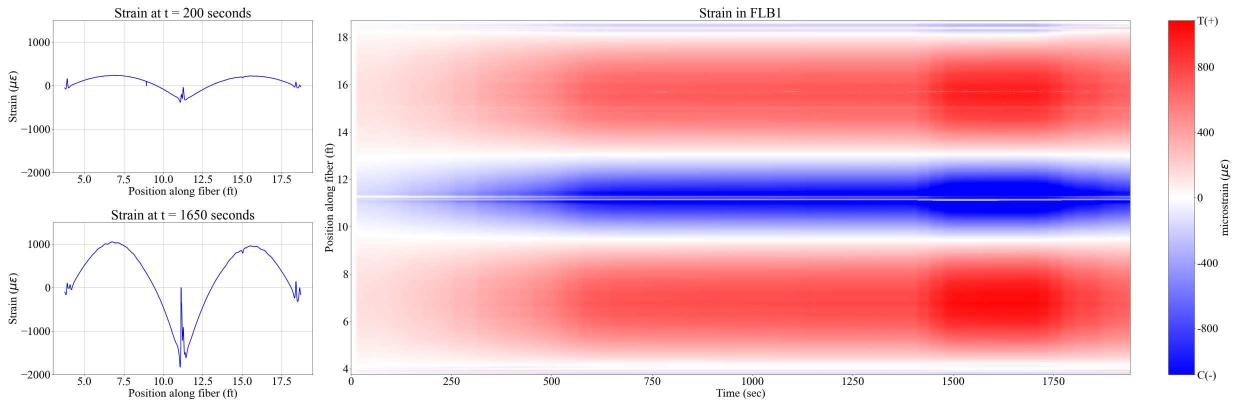

Figure 14: Strain distribution obtained from Fiber Optic Sensing for DT1

havior of the deck. Figure 14 and Figure 15 provide the strain distributions, obtained from distributed fiber optic sensing, of bottom flange FLB1 for both tests, illustrated in Figure 6 and Figure 7. The figures provide strain distributions during the initial stage and at the maximum pressure by showing the strain profile at two different applied pressures. The heat map (Fig. 14 and Fig. 15) exhibits strain distribution with red indicating tension and blue indicating compression. The position along fiber represents the longitudinal direction of the deck. For the first test (DT1), the strain distributions of the bottom flanges show global displacement behaviors, represented by tensile strain in the middle span between center support and end supports and compressive strain at the center support. For a two-span beam with support at the middle and both ends under uniform loading, the center support acts a negative moment region, hence the compressive strain at the center support. For the second test (DT2), the strain distributions along the bottom flanges exhibited the maximum tensile strain at the midpoint of the span, while minimal compressive and tensile strain were observed near the end supports. For a simply supported single-span beam, the bending moment is zero at the supports and maximum at the midpoint of the span. However, the regions near the supports experience bending moment gradients, resulting in both tensile and compressive strains at the bottom flange. Strain magnitude increased as the pressure increased. While strain gauges exhibit similar behavior, fiber optic sensing has demonstrated superior capability in capturing strain responses, as it is not limited to measuring strain in discrete locations but rather continuously along the fiber length. Strain magnitude increased as the pressure increased. While strain gauges exhibit similar behavior, fiber optic sensing has demonstrated superior capability in capturing strain responses, as it is not limited to measuring strain in discrete locations but rather continuously along the fiber length.

3.2 Displacement results

3.2.1 Results from OptiTrack

Global displacements can be quantified by tracking the displacement of reflective markers using infrared optical tracking cameras. Figure 16 provides the vertical displacement of the deck for initial loading condition and maximum pressure loading for three tests, measured by optical tracking system. Vertical displacement results for a top flange and a bottom flange for each test setup are shown in the figure. In the first test (DT1), vertical displacements measured by the optical tracking

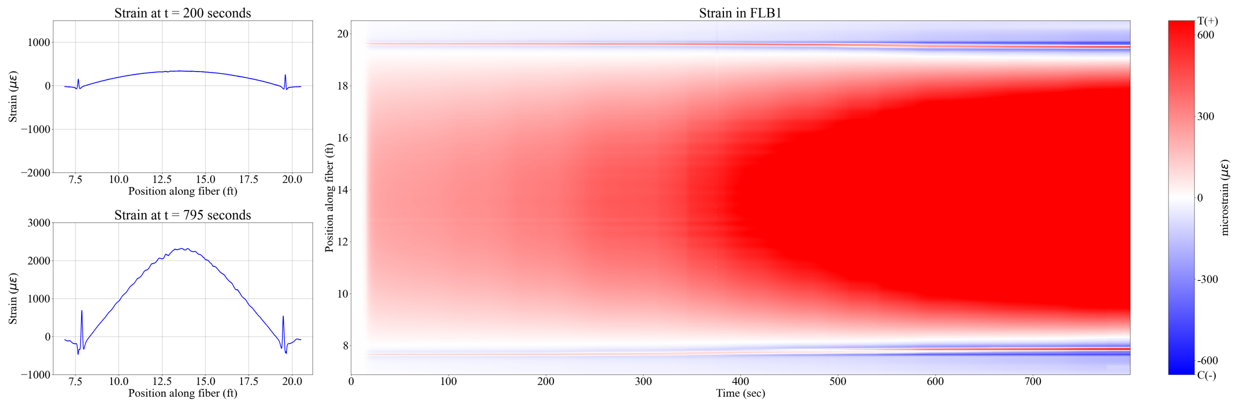

Figure 15: Strain distribution obtained from Fiber Optic Sensing for DT2

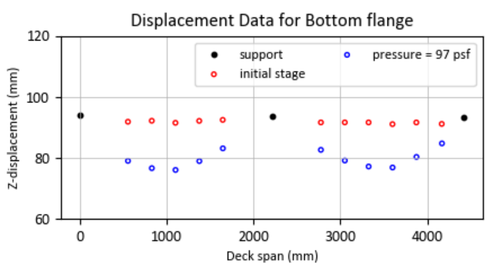

(a) Displacement data for bottom flange(DT1)

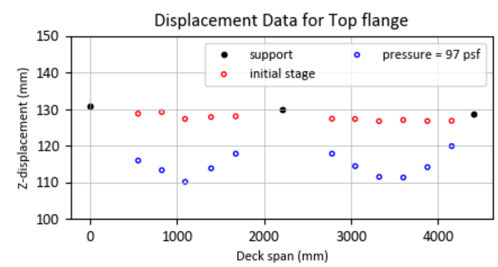

(b) Displacement data for top flange(DT1)

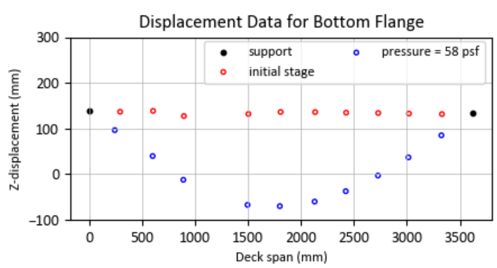

(c) Displacement data for bottom flange(DT2)

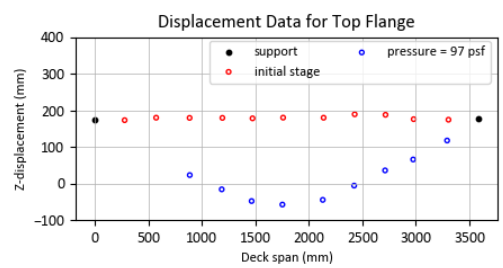

(d) Displacement data for top flange(DT2)

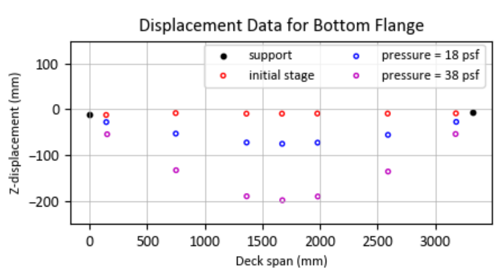

(e) Displacement data for bottom flange(DT3)

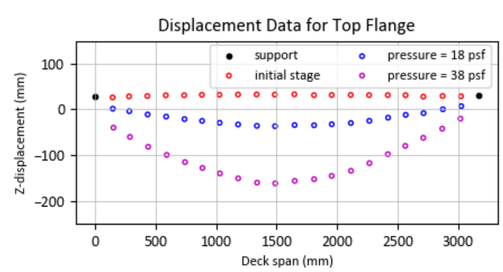

(f) Displacement data for top flange(DT3)

Figure 16: Vertical Displacement measured by OptiTrack

system were 9.54 mm (0.38 in) for the top flange and 12.5 mm (0.49 in) for the bottom flange. In the second and third tests (DT2 and DT3), the corresponding displacements were 237.5 mm (9.35

in) and 195.9 mm (7.71 in) for DT2, and 194.1 mm (7.64 in) and 189.25 mm (7.45 in) for DT3. Due to the presence of a center support in the first test (DT1), the vertical displacement measured of the deck measured by Optitrack system was significantly lower compared to second test (DT2) and third test (DT3), despite first test (DT1) being subjected to the highest pressure loading among the three tests. These results demonstrate that the optical tracking system can be an effective tool for accurately capturing three-dimensional deformations under varying loading conditions.

3.2.2 Results from Fiber Optic Sensing

Figure 14 and 15 illustrate the global buckling behavior of a steel deck measured using fiber optic sensors installed on the bottom flanges. The global buckling deformation is quantified by integrating strain along the fiber optic sensing length across the deck span. Strain ε is defined as the relative change in length, $\varepsilon = \frac{\Delta L}{L_0}$, which can be rearranged to compute the length change as:

$$\Delta L = \varepsilon \times L_0$$

The total length change is obtained by summing the strain contributions over the gauge length, expressed as:

$$\Delta L_{\text{total}} = \sum \varepsilon_i \cdot L_i$$

where ε_i is the strain at segment i and L_i is the corresponding segment length. By adding this change in length to the initial length, the deformed length of the deck can be determined at each time step. This process is repeated throughout the experiment to track the progressive deformation until the final deformed length is obtained. Based on this deformed length, global buckling displacements can be evaluated. Two key assumptions were made in this analysis: first, the support conditions during the experiment were considered simply supported, and second, the deflected shape of the steel deck was assumed to follow a sine curve. Using the deformed length as the arc length of the sine curve, the maximum deflection at mid-span was derived for both single-span and double-span configurations.

Figure 17 presents the vertical displacement of the deck measured using fiber optic sensing and the optical tracking system during the first test (DT1) under initial loading and maximum pressure conditions. Bottom flange FLB1 for first test setup and bottom flange FLB2 for second test setup were considered for this analysis (Figures 6 and 7). For DT1, the maximum vertical displacement recorded by fiber optic sensing was 23.23 mm (0.91 in) for the left span and 22.25 mm (0.88 in) for the right span. In comparison, the optical tracking system measured 22.14 mm (0.87 in) for the left span and 21.45 mm (0.84 in) for the right span. The percentage difference between the two methods was 4.70% and for the left span and 3.6% for the right span. For the second test (DT2), the maximum vertical displacement recorded by fiber optic sensing and the optical tracking system was 172.83 mm (6.8 in) and 177.36 mm (6.98 in), respectively, with a percentage difference of 2.5%. These minor discrepancies indicate a strong correlation between the fiber optic sensing and optical tracking systems. Overall, both methods demonstrate consistent agreement in measuring vertical displacement, with only slight variations observed.

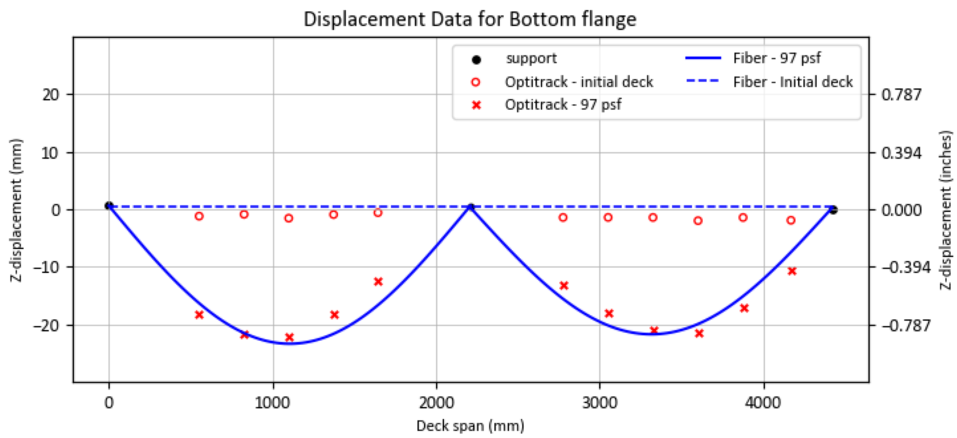

(a) Test DT1

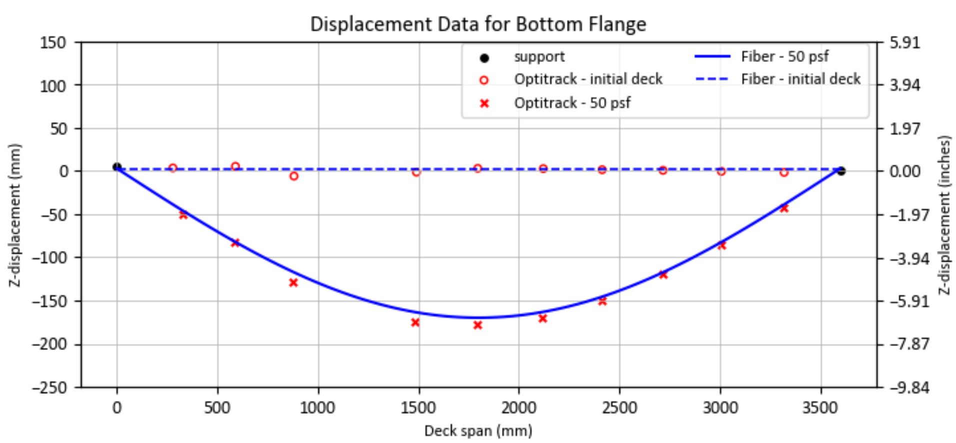

(b) Test DT2

Figure 17: Vertical Displacement measured by Fiber Optic Sensing and Optical Tracking System

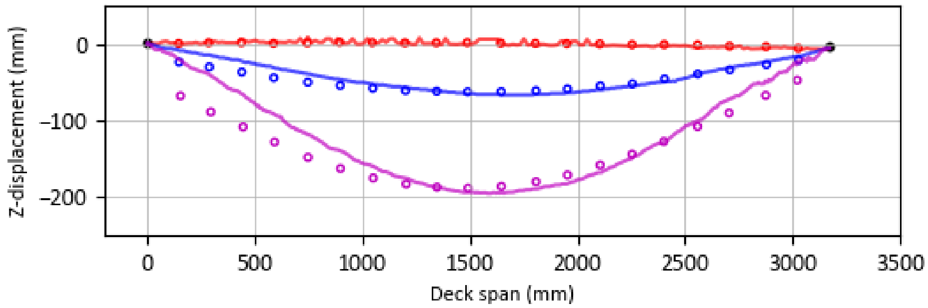

(a) Top flange FT31

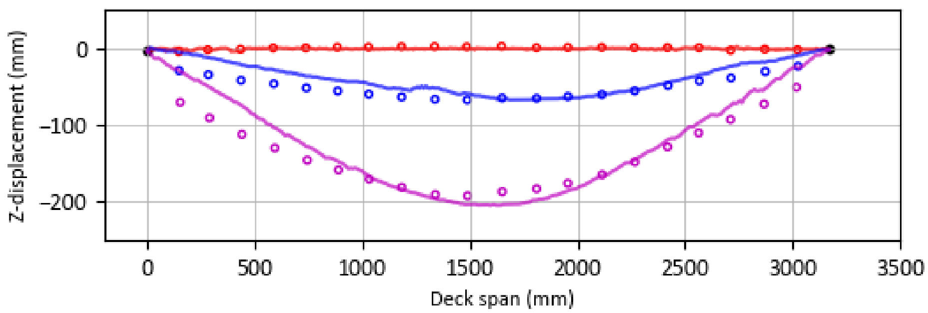

(b) Top flange FT32

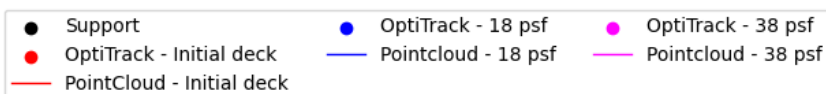

Figure 18: Vertical Displacement measured by OptiTrack and PointCloud

3.2.3 Results from PointCloud

For the third test setup, DT3, pointcloud scans were taken for pressure loadings of 18 psf and 38 psf using an Apple iPad Pro equipped with a LiDAR camera. The initial unloaded stage of the deck was captured by Artec Ray Scanner. Figure 18 shows the vertical displacements of the initial deck (no pressure loading) and under pressure loadings of 18 psf and 38 psf for flanges FT31 and FT32 of deck test DT3. Both the iPad point cloud and the OptiTrack system successfully captured the anticipated deflection profile of simply supported beam, with maximum displacement occurring at the center of the span and zero displacement at the supports. For top flange FT31, at 18 psf the maximum displacement measured by the optitrack system and iPad pointcloud is 62.53 and 65.01 mm, respectively, with a percentage difference of 3.8%. For the same top flange, at 38 psf, the maximum displacement measured by the optitrack system and the iPad pointcloud is 188.47 and 195.25 mm, respectively, with a percentage difference of 3.47%. For top flange FT32, at 18 psf maximum displacement measured by optitrack system and iPad pointcloud is 67.36 mm and 67.23 mm, respectively, with a percentage difference of 0.19%. For same top flange, at 38 psf, maximum displacement measured by optitrack system and iPad pointcloud is 192.37 mm and 203.59 mm, respectively, with a percentage difference of 5.51%. As shown in Figure 18, the vertical displacements measured by the OptiTrack system and the iPad point cloud do not perfectly align with each other. The top of the deck is covered by plastic tarp and the scanner had to scan the deck through the plastic tarp. At low pressure, some of the plastic sheet remain loosely fitted to the deck. Consequently, point cloud scans captured under these conditions tend to underestimate the displacement of the deck. But as the pressure increases, the sheet progressively tightens and conforms more closely to the deck surface. Point cloud scans captured at higher pressure more accurately reflect the vertical displacement, closely aligning with OptiTrack system measurement. Despite the limitations, both iPad point cloud and OptiTrack system have measured vertical displacement effectively, providing accurate and reliable data for steel deck deflection under pressure loadings.

4 Discussion

Global buckling behavior of a steel deck with varying support conditions under pressure loadings was investigated in this study. Innovative measurement techniques such as Fiber Optic Sensing, Point Cloud Scanning, and Optical Tracking System along with traditional strain gauges were employed. The first test, DT1, was conducted to validate the newly developed experimental apparatus, the SEAhorse Vacuum Box, and to assess the performance of the instrumentation, including fiber optic sensing and the OptiTrack system, under pressure loading. The second test, DT2, extended the validation by utilizing fiber optic sensing and the OptiTrack system to monitor a single-span configuration up to failure. With the success of these two experiments, the third test, DT3, introduced a point cloud technique using iPad LiDAR scanning, applied to the same setup and instrumentation methods as the second test, to further explore its capabilities within the experimental framework.

Fiber Optic Sensing effectively measured strain distribution of the steel decks for all three cases. The strain distribution of the steel deck obtained from fiber optic sensing suggests that this technique can be used to assess the behavior of the steel deck system. Global buckling behavior can be assessed through the strain results of the bottom flanges, while the local buckling behavior is primarily reflected in the strain measurements of the top flanges as shown in Koh et al. (2024). Both fiber optic sensing and strain gauges have provided identical strain profiles: compressive strain at supports and tensile strain at midspan. Moreover, fiber optic sensing offers continuous, distributed strain data along the entire length of the fiber, overcoming the limitations associated with traditional strain gauges, which are typically placed at a limited number of points along the span.

The OptiTrack system was employed to measure the vertical displacement of the steel deck under varying support conditions and different pressure loadings. The results obtained from the OptiTrack system successfully captured the expected deflected shapes of both the simply supported beam and the two-span beam with a center support. Fiber optic sensing measures strain along the cable, which can be used to estimate vertical deflections. The deflection is calculated based on an assumed deflection profile, which in this case was a sine curve between supports. In this study, the assumed deflection profile resulted in good comparisons to the OptiTrack displacements, showing that fiber optic sensing can be a useful tool for measuring structural behavior and displacements. Furthermore, the results from the point cloud scans not only successfully captured the expected deflection curve but also closely aligned with the measurements obtained from the OptiTrack system, demonstrating a high level of accuracy and reliability. In future studies, iPad LiDAR scans can be integrated to complement the real-time tracking of strain accumulation and deformation captured through fiber optic sensing, providing a comprehensive approach to monitoring structural behavior. In scenarios where the installation of cameras and markers is impractical, fiber optic cables can be easily adhered to the structure, offering a flexible and efficient alternative for displacement measurement.

5 Conclusions

Profiled steel deck was loaded with uniform pressure inside a vacuum box in single span and double span configurations. Multiscale strain was measured using distributed fiber optic sensing, infrared optical tracking, and point clouds obtained from photogrammetry and LiDAR to determine if the instrumentation could capture and quantify global buckling and deformation behavior. Distributed fiber optic sensing, with its higher spatial resolution, enables the identification of subtle strain gradients and localized phenomena that conventional strain gauges may fail to capture.

It was found that distributed fiber optic sensing provided continuous longitudinal strain measurements along the deck flanges which illustrated the overall deck behavior. Furthermore, the longitudinal strain could be converted to vertical displacements using a correctly assumed displacement profile. Vertical displacements were also determined through the Scaniverse app on an Apple iPad Pro which used the built-in LiDAR sensor and photogrammetry to create a low-density point cloud. Both these techniques compared well to the vertical displacements measured by the Optitrack system, which used infrared optical tracking to measure 3D displacements. Incorporation of these innovative measurement techniques offers a comprehensive framework for analyzing the behavior of steel decks under pressure loading. These technologies enable precise monitoring and characterization of structural deformations, providing valuable insights into the mechanics of buckling phenomena. The findings of this study will lay the groundwork for enhancing structural assessments.

6 Acknowledgments

The Vacuum Box chamber known as SEAhorse (Suction Experimental Apparatus), was funded by the Steel Deck Institute, with material donations from Canam Steel Corporation, DACS, Inc., Gooder-Henrichsen Co., New Millennium, Nucor Corporation, and Simpson Strong-Tie. Funding for the fiber optic sensing portion of this research project was provided under a Cooperative Agreement with the U.S. Army Corps of Engineers, Engineer Research and Development Center, Construction Engineering Research Laboratory (USACE ERDC-CERL). The authors would also like to thank the amazing research team, especially Gabriel Lepak, former graduate project assistant, and Lennart Fredrik Schmitz and Quincy Eaton, undergraduate research assistants, for their assistance with the experiments.

References

ASTM E8/E8M-13a (2015). *Standard Test Methods for Tension Testing of Metallic Materials*. Standard. DOI: 10.1520/E0008_E0008M-13A.

Chen, Shen-En et al. (2012). "3D LiDAR Scans for Bridge Damage Evaluations". en. In: *Forensic Engineering 2012*. San Francisco, California, United States: American Society of Civil Engineers, pp. 487–495. ISBN: 978-0-7844-1264-0. DOI: 10.1061/9780784412640.052.

He, Xinyi et al. (2023). "Experimental study on buckling behavior of orthotropic steel deck with slender open ribs for large span suspension bridges". In: *Journal of Constructional Steel Research* 201, p. 107681. ISSN: 0143-974X. DOI: 10.1016/j.jcsr.2022.107681.

Huang, Yuner and Ben Young (2014). "The art of coupon tests". In: *Journal of Constructional Steel Research* 96, pp. 159–175. ISSN: 0143-974X. DOI: 10.1016/j.jcsr.2014.01.010.

Jo, Hyeon Cheol et al. (2018). "Non-contact strain measurement for laterally loaded steel plate using LiDAR point cloud displacement data". In: *Sensors and Actuators A: Physical* 283, pp. 362–374. ISSN: 0924-4247. DOI: 10.1016/j.sna.2018.09.012.

John, Keerthana et al. (2020). "Experimental Investigation of Novel Corrugated Steel Deck under Construction Load for Composite Slim-Flooring". en. In: *Buildings* 10.11. Number: 11 Publisher: Multidisciplinary Digital Publishing Institute, p. 208. ISSN: 2075-5309. DOI: 10.3390/buildings10110208.

Kalybek, Maksat, Mateusz Bocian, and Nikolaos Nikitas (2021). "Performance of Optical Structural Vibration Monitoring Systems in Experimental Modal Analysis". en. In: *Sensors* 21.4. Number: 4 Publisher: Multidisciplinary Digital Publishing Institute, p. 1239. ISSN: 1424-8220. DOI: 10.3390/s21041239.

Kechavarzi, Cedric et al. (2016). *Distributed Fibre Optic Strain Sensing for Monitoring Civil Infrastructure*. Ed. by Nicholas de Battista et al. ICE Publishing. DOI: 10.1680/dfossmci.60555.

Koh, Hyeyoung et al. (2024). "Buckling Detection of Profiled Steel Deck Using Strain Measurement Techniques in a New Vacuum Box Apparatus". In: *Proceedings of the Annual Stability Conference*. Structural Stability Research Council. San Antonio, Texas: Structural Stability Research Council. URL: https://files.ssrcweb.org/proceedings/2024/Koh_et_al_SSRC_2024.pdf.

Lawson, R. Mark and Sunday Popo-Ola (2013). "Load capacity of continuous decking based on small-scale tests". In: *Thin-Walled Structures* 69, pp. 79–90. ISSN: 0263-8231. DOI: 10.1016/j.tws.2013.03.011.

Liang, Dun et al. (2024). "Experimental investigation of global-distortional interaction buckling of stainless steel C-beams". In: *Journal of Constructional Steel Research* 214, p. 108472. ISSN: 0143-974X. DOI: 10.1016/j.jcsr.2024.108472.

Optitrack (2021). *Motive*. Version Motive 3.0.2. URL: http://optitrack.com/software/motive/index.html.

Park, S.W. et al. (2015). "3D displacement measurement model for health monitoring of structures using a motion capture system". en. In: *Measurement* 59, pp. 352–362. ISSN: 02632241. DOI: 10.1016/j.measurement.2014.09.063.

Raebel, Christopher and Dawid Gwozdz (2020). "Experimental and Numerical Comparison of Flexural Capacity of Light Gage Cold Formed Steel Roof Deck". In: *American Iron and Steel Institute (AISI) Specifications, Standards, Manuals and Research Reports (1946 - present)*. URL: https://scholarsmine.mst.edu/ccfss-aisi-spec/221.

Rajan, Gangadhara and Badri G. Prusty, eds. (2016). *Structural Health Monitoring of Composite Structures Using Fiber Optic Methods*. 1st. CRC Press. DOI: 10.1201/9781315369815.

Scaniverse Inc. (2024). *Scaniverse*. Version Scaniverse 4.0. URL: https://scaniverse.com/.